IOP Conf. Series: Materials Science and Engineering **444** (2018) 022006 doi:10.1088/1757-899X/444/2/022006

Scalable Wind Turbine Blades nondestructive evaluation using different types of sensors

N Iftimie[1], R Steigmann[1], G S Dobrescu[1], N A Danila[1,2], A Savin[1*], P D Barsanescu[2], V Goanta[2]

[1]Nondestructive Testing Department, National Institute of R&D for Technical Physics, Iasi, Romania
[2]Mechanical Engineering, Mechatronics and Robotics Department, "Gheorghe Asachi" Technical University of Iasi, Romania

E-mail: asavin@phys-iasi.ro

Abstract. The most important part of wind turbine is the blade that must be tested during fabrication and functioning when can be damaged by moisture absorption, fatigue, wind gusts or lightning strikes. The common defects in turbine blades may be faulty microscopic and mesoscopic appeared in matrix, broken fibers can also appear and develop under moderated loads, or cracks and delaminations due to low energy impacts, etc. The paper propose to present the results obtained from testing and monitoring of a scalable wind turbine blade using different sensors placed on critical location which were determined by finite element method simulation. A comparison between the complementary methods is carried out.

1. Introduction

Most of the past years papers are focused on optimizing wind turbine (WT) design parameters to minimize energy costs, maximize energy production, minimize wind turbine blades (WTB) sizes [1-6]. This optimization resulted in slender blades with less resistance. All these had implications over the blade profile and lead to rethinking of the weight and the stability of the blade. In order to obtain greater efficiency and to increase the generated power, the general trend is to use large-diameter rotors and manufacturing the blades with glass fiber-reinforced plastics (GFRP) due to their low weight. The blades are usually subject to random and complex mechanical stresses. Some papers [7] studied major design cases, meanwhile others [8] were focused on cases with loadings in the design of blades and the evaluation of their deformations.

In the process of optimizing the structural design of the blade, the priority is to prevent failure in compliance with the structural resistance requirements. Critical areas were taken into account when optimizing the blade [9] selecting the Tsai-Wu failure criterion. It can be concluded that the decision to maximize the aerodynamic performances to optimize the objective functions of the wind turbine has to be done according to the safety in operation rules, with the aim of minimum report cost of energy /maximum annual energy production. Chehouri, et all [10] highlights the need to further study the issues that have not been resolved satisfactorily: complete load calculation and composite structural optimization. Nondestructive testing techniques for in-service inspection and the determination of high risk degradation regions of blades are growing, function of the type and the blade dimension, being based on numerous studies and researches. The nondestructive testing must be carried out both during the fabrication process as well as during the functioning of the blades, first for the decreasing of

fabrication and maintenance costs and for reduced downtime. These explain the attention given to structural health monitoring (SHM) systems for WTB, development and consolidation of diagnosis, prognosis methodologies, damage detection (location and their nature) [11-13]. The SHM process involves the observation of a system over time using periodically sampled dynamic response measurements from an arrangement of sensors, the extraction of damage-sensitive features from these features to determine the current state of system health. In the process of optimizing the structural design of the blade, the priority is to prevent failure in compliance with structural resistance requirements. Figure 1 illustrates the SHM system concept [8], the blades damages shall be detected and evaluated with high probability of detection and reliability coefficient.

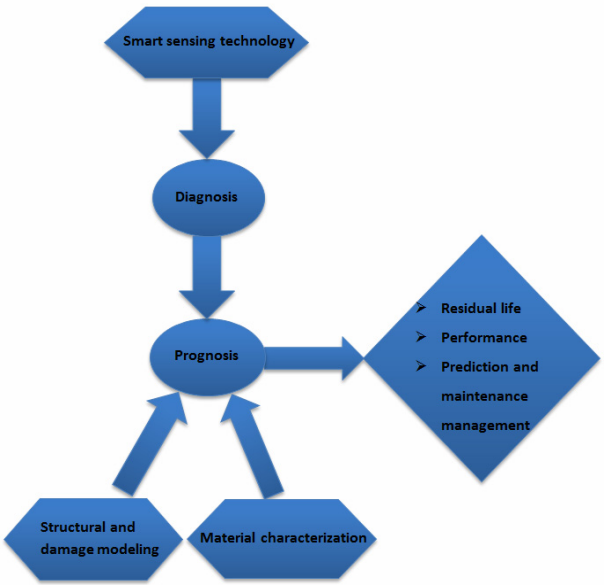

Figure 1. SHM system

For an estimated lifetime of 20 years and extended as long as is possible, the long-term integrity of a blade became a very interested area. The monitoring of WTB made from GFRP have been reviewed in [7], proposing either statistical pattern recognition using simulation or experimental data, or in [14] considering mechanical property testing and full-scale testing as well as nondestructive testing methods. In order to calculate the lifetime of GFRP structures used in WTB construction, it is essential to have access to information about the fatigue resistance of the material. These data include a number of fatigue tests in the frame of specific combinations of amplitude and average stress.

Different databases were compiled, regarding extended fatigue of GFRP in WTB [15, 16], the results between different materials and the loading conditions are not transferable, being necessarily further high experimental effort for each new project and used material. There are many literature reviews concerning WTB starting from design, propulsion and including theories of maximum efficiency [17-20]. In order to decrease the fabrication and maintenance costs, as well as for avoiding unproductive time, NDT is required both during fabrication and in-service. The nondestructive testing (NDT) techniques for in-service inspection and determination of regions with high degradation risks are developed (function on the type and the size of the WT) [21].

The results of complex mechanical tests, performed on scalable WTB model (in our case a blade of 1750 mm length) are used to give efficiency to monitoring strategy. Using FEM, the maximum stress zones [22] and damage evolution and remnant stress [23] have been determined.

The paper presents results of testing of a WTB, static loading in static conditions, using three types of sensors (i.e. wireless sensor (WRS), optical fiber (OF) Fiber Bragg Gratings (FBG), stress/strain gauges (SG)) in order to monitor possible damages that further can be transformed into flaws. To the best of our knowledge, this investigation has not been performed for WTBs before.

2. Principles

The composite structures are designed and realized based on the concept that a layered structure more easily supports an early stage damage that can be stopped when it has a tendency to propagate following the repeated loads prescribed by the project. Based on a priori knowledge about WTB, the sensors used for their characterized are distributed according to the most expected damage area, aiming the minimizing of the sensors number.

2.1 Sensors with Fiber Bragg Grating (FBG)

SHM includes the use of FBG for detecting delamination in composite laminates [24] and monitor impact event occurrence [25,26]. A FBG is a periodic or semi periodic permanent perturbation of the fiber core refractive index. Optical fiber (OF) sensors are made based on OF in integrated structures. This sensor can monitor the structure in critical regions. The central wavelength of this signal, called Bragg wavelength λ_B is related to the physical parameters of the grating according to $\lambda_B = 2n\Lambda$ where n is the effective refractive index of the fundamental mode propagating inside the fiber; Λ is the spacing between gratings, known as grating period.

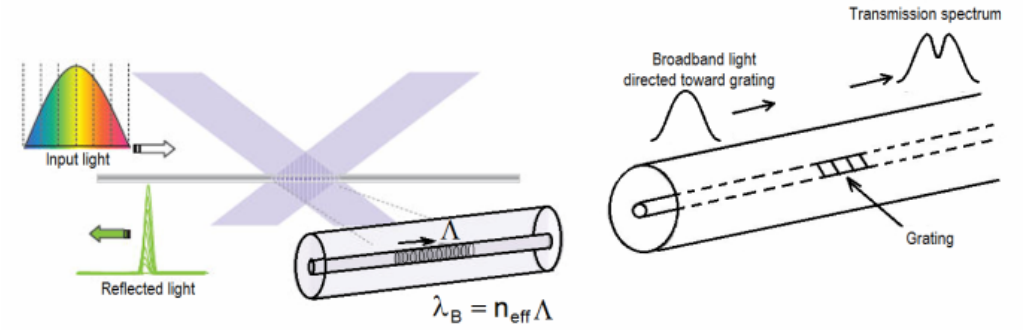

Figure 2. Fiber Bragg gratings principle [26]

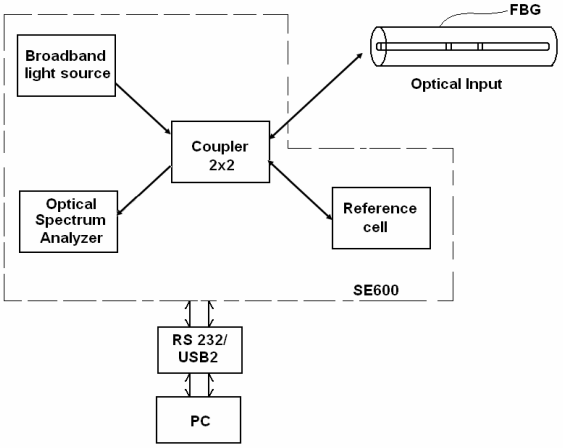

Figure 3. Basic diagram and equipment of FBG interrogator

When the fiber containing OF is submitted to strain, the central wavelength is displaced to higher or smaller values [27]. The direction and the magnitude of displacement are proportional with the modification of strain or temperature. The strain axial sensitivity is $d\lambda_B/d\varepsilon \approx \lambda_B(1-p_e)$ where $\partial\lambda_B$ is the OF wavelength shift $\varepsilon \ll 1$, p_e is photo-elastic coefficient of the fiber $p_e \approx 0.22$, OF sensors whose gauge lengths are about 10 mm were used for SHM.

$$\frac{\partial\lambda_B}{\lambda_B} \approx (1-p_e)\varepsilon; \quad \frac{\partial\lambda_B}{\lambda_B} \approx (1-p_e)\varepsilon; \quad \frac{\partial\lambda_B}{\lambda_B} \approx 0.78\varepsilon; \tag{1}$$

The OF strain sensing can be expressed as $\varepsilon = \frac{1}{0.78\times10^{-6}}\frac{\Delta\lambda_B}{\lambda_B}$. In structure of WTB, 3 OF sensors were embedded along the central longitude of the blade, placed into critical points determined by FEM of blade under bending. The optical block diagram of measurement is show in Figure 3.

2.2 Wireless sensors

The passive WRS designed to monitor stress/strain status have as sensitive element that follows the relative displacement (in compression or tension) of its components due to loads. In specific construction as 2D geometry on flexible support, copper SRR can be used as stress/strain sensors [28, 29]. The sensor consists in a folded rectangular microstrip patch antenna [30] coupled with a tunable inductive SRR and with a passive IC chip. The structure of this sensor is shown in Figure 4a, the sensing element is shown in Figure 4b. The resonance frequency of sensor is in range of RF and microwaves, depending of geometrical dimensions and design, for a quality factor of the equivalent circuit between tens - hundreds. WRS [31] presents resonant properties [32] and the inductance and the capacitance are given by [33]. The resonance frequency is $f_r = c/4(L+\Delta L)\sqrt{\varepsilon_r}$ with c speed of light in vacuum, L the length of the copper layer, ε_r the dielectric permittivity of the substrate, ΔL is the additional length who compensate the effect due to thickness, width and dielectric constant of the substrate. Parallel with the capacitance C, a capacitive element sensitive to stress/strain is connected, with the capacitance varying linear with the strain as $C_{sensitive} = \varepsilon_r\varepsilon_0 w_1 g/u(1+\varepsilon_s)$ with u thickness of dielectric layer and strain in $\mu m/m$.

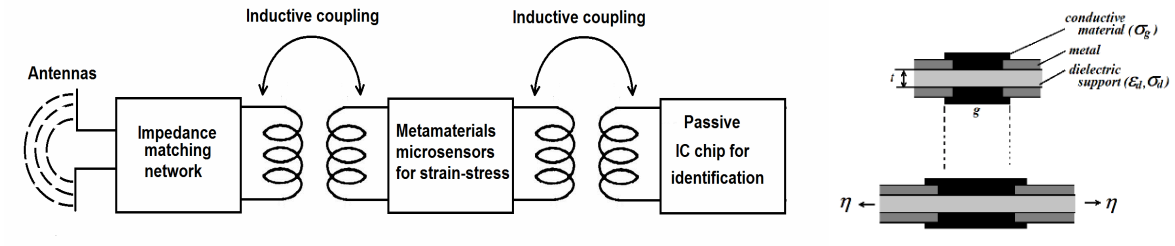

(a) (b)

Figure 4. Metamaterial passive wireless sensors for SHM: a) schematic of a RF/microwave–RFID tag; b) schematic of sensing element

For the capacitive element, sensitive to stress/strain, to function upon a law closer to this, it is imposed that the Poisson ratio of dielectric support shall be as high as possible. For polyimide, the layer supporting copper strips, the Poisson ratio is 0.4. If $\varepsilon_s = 10\,\mu m/m$, the connection between the two-capacitance make C increases with 10%, inductance L remaining unchanged. Detection system consist in a RFID reader and a RFID tag [33], the tag including the sensor and the integrate circuit (IC). When the sensor detect a modification of the strain ε, the frequency is

$$f_r^{'} = \frac{c}{4(1+\varepsilon)(L+\Delta L)\sqrt{\varepsilon_r}} = \frac{f_r}{1+\varepsilon} \approx f_r(1-\varepsilon) \tag{2}$$

For a small load, the resonance frequency modifies almost linear with load, the load can be determined if the resonance frequency is measured. The RFID tag antenna assures that the interrogation frequency f shall be equal with the one of RFID tag to obtain perfect matching of impedance between antenna tag and IC chip. The smallest amount of energy must be transmitted toward reader to activate RFID tag, the transmitted power threshold (measured through the reader) reach minimum value at resonance frequency.

2.3 Strain Gauges

Three-element strain gage rosette must be employed to determine the principal strains in a general biaxial stress state when the directions of the principal axes are unknown. The usual goal of

experimental stress analysis, however, is to arrive at the principal stresses, for comparison with some criterion of failure [34]. This form of rosette offers the following advantages in such cases: thin and flexible, with greater conformability to curved surfaces; minimal reinforcing effect; superior heat dissipation to the test part; available in all standard forms of gage construction, and generally accepts all standard optional features; optimal stability; maximum freedom in lead wire routing and attachment.

The equations for calculating principal strains from three rosette strain measurements are derived from what is known as a "strain-transformation" relationship. For each gauge, maximum and minimum specific strains ε_{max}, ε_{min}, the arbitrary angle θ from the major principal axis, maximum shear strain γ_{max}, maximum and minimum normal stress, σ_{max}, σ_{min}.

$$\varepsilon_{max} = \frac{1}{2}\left[\varepsilon_a + \varepsilon_b + \sqrt{2\left(\varepsilon_a - \varepsilon_b\right)^2 + \left(\varepsilon_b - \varepsilon_c\right)^2}\right] \tag{3}$$

$$\varepsilon_{min} = \frac{1}{2}\left[\varepsilon_a + \varepsilon_b - \sqrt{2\left(\varepsilon_a - \varepsilon_b\right)^2 + \left(\varepsilon_b - \varepsilon_c\right)^2}\right] \tag{4}$$

$$\theta = \frac{1}{2} arctg\left[\frac{2\varepsilon_b - \varepsilon_a - \varepsilon_c}{\varepsilon_a - \varepsilon_c}\right][rad] \quad ; \quad \gamma_{max} = \sqrt{2\left(\varepsilon_a - \varepsilon_b\right)^2 + \left(\varepsilon_b - \varepsilon_c\right)^2} \tag{5}$$

$$\sigma_{max} = \frac{E}{2\left(1-\nu^2\right)}\left[\left(1+\nu\right)\left(\varepsilon_a + \varepsilon_c\right) + \left(1-\nu\right)\sqrt{2\left[\left(\varepsilon_a - \varepsilon_b\right)^2 + \left(\varepsilon_b - \varepsilon_c\right)^2\right]}\right] \tag{6}$$

$$\sigma_{min} = \frac{E}{2\left(1-\nu^2\right)}\left[\left(1+\nu\right)\left(\varepsilon_a + \varepsilon_c\right) - \left(1-\nu\right)\sqrt{2\left[\left(\varepsilon_a - \varepsilon_b\right)^2 + \left(\varepsilon_b - \varepsilon_c\right)^2\right]}\right] \tag{7}$$

$$\tau_{max} = \frac{E}{2\left(1+\nu\right)}\left[\sqrt{2\left[\left(\varepsilon_a - \varepsilon_b\right)^2 + \left(\varepsilon_b - \varepsilon_c\right)^2\right]}\right] \tag{8}$$

3. Experimental Set-up

Detecting early-stage WTB degradations and monitoring their progress over time can lead to improved diagnostic capability and the development of more efficient repair strategies and, last but not least, the improvement of structural blade design. Taking into account the efficacy of the method and a priori knowledge about WTB (obtained by simulations), the sensors is distributed on the most expected damage area, aiming the minimizing of the sensors number (Figure 5 and Figure 6).

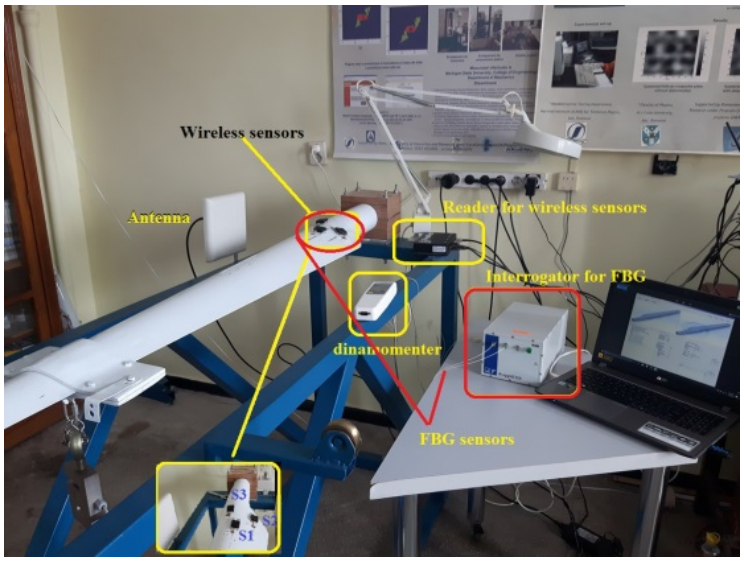

Figure 5. Testing stand for: wireless sensors and optical fiber measurements

The blade has been realized from E-glass/epoxy EPIKOTE Resin MGS LR 385 composite. The leading edge is straight and the trailing edge conical for an easy construction. The profile follows NACA airfoil. For increased structural strength and stiffness at 0.286R (R - the total length of distance between the center of rotor and the tip of blade), the same NACA has been applied both for the upper surface and lower surface, keeping the aerodynamically performances of the blade's tip. The profiles between 0.268R and tip were linear interpolated. A compromise has to be found between high-resolution and long propagation distance. Three sensors C2A-06-062WW-350, stacked rosette were used, each having 3 strain gauges with 350 Ω electrical resistances were employed (Figure 6a). These were connected to Vishay P3 Strain Indicator and Recorder, in quarter bridge connection with automatic balance. Their positioning (Figure 6b) has allowed the determination of deformations due to bending along blade axis at distance of 488mm from the fixed end, respectively close to trailing edge at 409mm from the fixed end, as well as closely to the leading edge at 351 mm from the hub. The bending tests were effectuated in 7 loading stages with 100N steps, with maximum of bending momentum of 900Nmm.

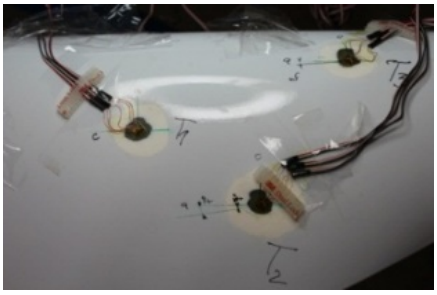

(a)

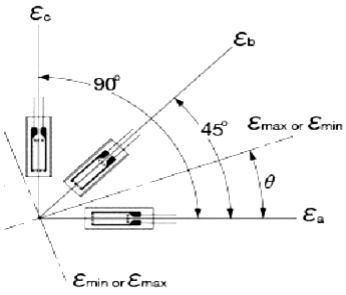

(b)

Figure 6. Strain gauges measurements: a) strain gauge; b) positioning of the stacked gauges

4. Experimental results and discussions

The simulation of blade behavior has been carried out with ANSYS Academic 17.2 at 300 mm distance from the tip of the blade, a compression force of 500 N has been applied on Y axis (blade upper shell) on 100 mm width surface. The produced displacement of the tip of is 30.082 mm. Figure 7a presents the division of the blade in critical regions, in Figure 7b is presented the loading forces disposition. The FEM model shown above takes into account the presence of the reinforcement structure, which's mass cannot be neglected, especially if one considers that the distance from the axis of rotation increase the inertia and can reduce the frequency associated with the first mode of vibration of WTB. Fortunately, the glass fibers employed makes the structure very rigid. OF sensors are placed in region at 307 mm, 362 mm, 406 mm from the hub fixing in stand. All the loadings are static and the sensors were placed in region of maximum critical points. The critical regions of WTB are established using FEM with 338842 nodes, 832563 elements, the dimension of an element being 8 mm.

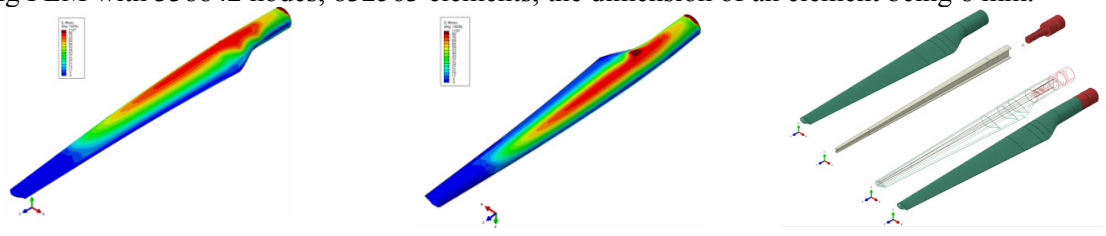

(a) (b)

Figure 7. FEM simulation of WTB: a) division of blade in critical regions; b) FEA assembly

The resulted maximum stresses were under material flow limit. In all the cases, the stresses on lower shell are higher than on the upper shell. The maximum stresses on WTB appear closely to the joint between the hub and the longeron and at transition between circular geometry to NACA profile. For the WRS the reader antenna is fixed on the upper part of the stand, at 30cm from the middle area

of WRS placement locus. The antenna is connected to a logger reader coupled to PC by USB. IC frequency range is [840÷960] MHz. The results of bending tests in a loading-unloading cycle are presented in Figure 6a and b. Maximum deformations at 700N loadings are characteristics of region where sensor S1 is placed (along longeron axis) and the minimums are in the region of sensor S2 (placed outside the critical zone). In addition, the deformation is linear, the loading remain in elastic range. During the unloading, the values follow the same characteristic as at loading. Comparing loading/unloading data at 500N with the simulated ones, it can be observed a good correlation of the displacement, experimentally being determined as 37 mm. The OF sensor, FBG single DTG S-01 type used for monitoring composite materials type GFRP [35] have center wavelength in 1535 nm with strain sensitivity and temperature sensitivity. This is connected at optical system FS22 Industrial BraggMETER HBM Germany coupled with PC. During the experiments, the temperature has been maintained constant at 22±1^{o}C. The experimental test setup was performed according to [36] progressively loading/unloaded forces were applied. Physically, the stress concentration around the damage in the composite laminates can be directly observed from the raw sensor signal.

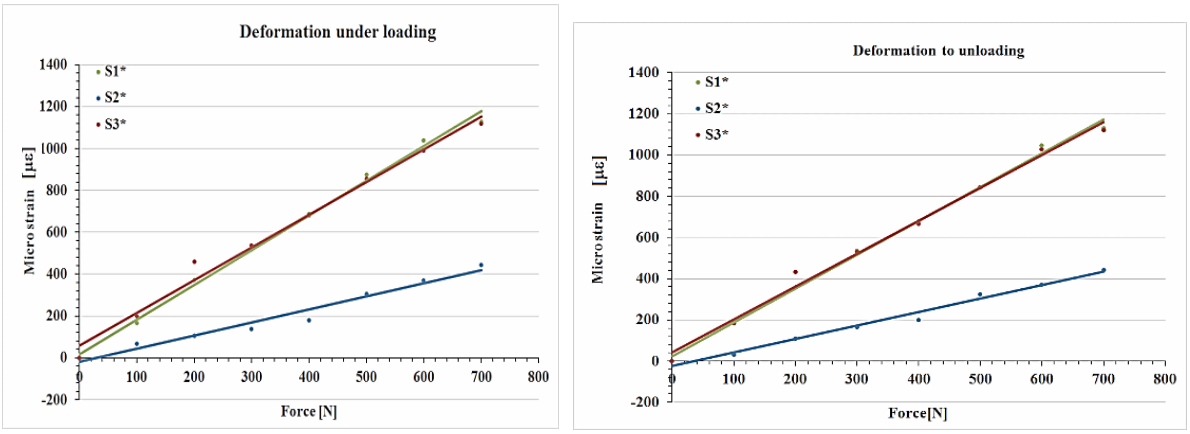

(a) (b)

Figure 8. Signal delivered by the WRS placed in critical regions of WTB: a) loading; b) unloading

The data is processed in Matlab 2014b, with the temperature correction. Figure 9a presents the raw data recorded by the device for different loadings. The relative variation of Bragg wavelength was determined in function of loading is presented in Figure 9b showing that the relative variation of Bragg wavelength is linear. The dependency strain-load for WTB in a loading-unloading cycle for three sets of experimental measurement is presented in Figure 9. The same linear dependency strain-load can be shown, even the existence of a remnant stress at force removal, indicating an accumulation of energy in WTB composite structure, preponderant in the resin. The measurements using OF were carried on the same time with those using WRS sensors. The sensor T1 measures the deformations of the blade in the plane of I shape longeron, having height/width variable along the blade, T2 measures the deformations of blade shell closely to the trailing edge and T3 measures the deformations of blade shell closely to leading edge.

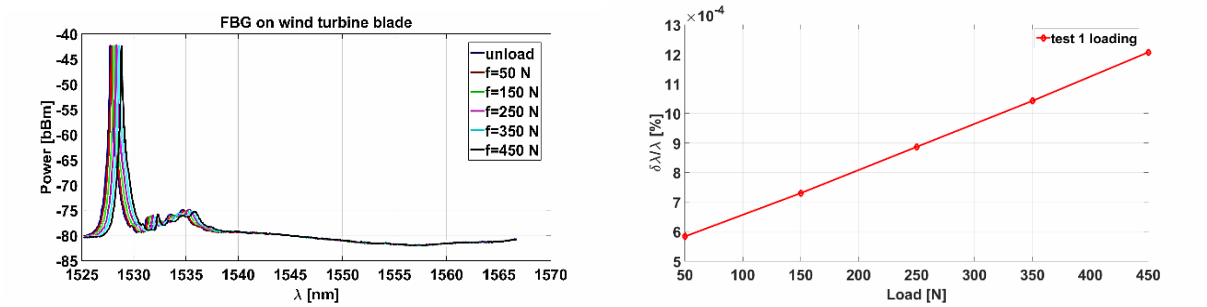

(a) (b)

Figure 9. FBG measurements: a) response to successive loading; b) relative variation of Bragg wavelength

The experimental data were used to calculate [37] maximum strain ε_{max}, minimum strain ε_{min}, acute angle from the axis θ, the maximum shear strain γ_{max}, maximum normal stress σmax, minimal normal stress σmin and maximum shear stress τmax using eqs. (3-9).

Figure 10 presents the plotting of σ_{max}, σ_{min} and τ_{max} for the 3SG for loading (Figure 10a,c,e) and unloading (Figure 10b,d,f) until maximum force of 700N. It can be observed that the high values of stresses with applied force appear in the region where sensor T3 is placed, this region being emphasized in FEM analysis too. The plots following the same profile shows that the tests were carried out in elastic range.

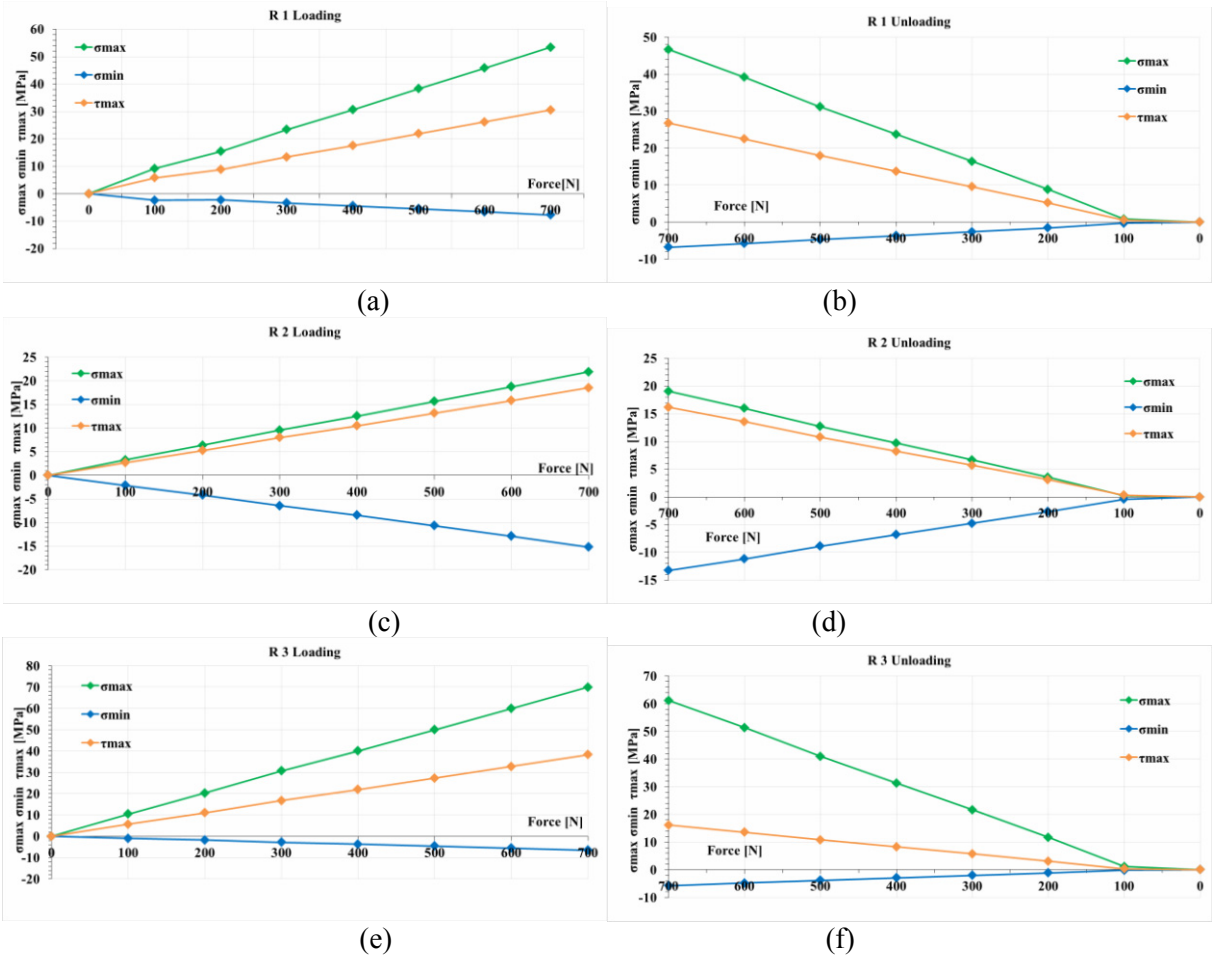

(a) (b)

(c) (d)

(e) (f)

Figure10. Variation of stresses with force: a) rosette 1 – loading; b) rosette 1 – unloading; c) rosette 2

– loading; d) rosette 2 – unloading; e) rosette 3 – loading; f) rosette 3 - unloading

5. Conclusions

We have use of three type of sensors to detect broken fibers which may occur and develop under moderated loads, or cracks and delamination due to low energy impacts, etc.
In order to avoid environmental disasters, it is necessary to establish diagnosis and prognosis methods, based on using information obtained from sensors constructed on known physical principles.
The monitoring is close related with nondestructive evaluation and the trend is to obtain real time information. Scalable WTB have been constructed and tested to loadings using WRS, OF-FBG and SG located in the maximum concentration stress zones.

The tests were carried on scalable models, in the further research the WRS sensors will be embedded, because in the frame of the project that sustains the paper, the blades will be employed into a demonstrator to show the righteous of solutions, reliability of correct diagnosis probability, prognosis, and evaluation of residual lifetime and maintenance management.

6. References

[1] Wind Energy Targets for 2020 – 2030, EWEA, 2011.
[2] http://www.ge-energy.com/products_and_ services/products/wind_turbines/ ge_1.5_77_wind_turbine.jsp
[3] http://rwea.ro/cifre-cheie/
[4] Negm HM and Maalawi KY 2000 Structural design optimization of wind turbine towers *Computers & Structures*, 74(6) pp 649-666
[5] Kusiak A and Song Z 2010 Design of wind farm layout for maximum wind energy capture *Renewable Energy* 35(3) pp 685-694
[6] Walford CA 2006 Wind turbine reliability: understanding and minimizing wind turbine operation and maintenance costs *No. SAND2006-11. Sandia National Laboratories*
[7] Kong C, Bang J and Sugiyama Y 2005 Structural investigation of composite wind turbine blade considering various load cases and fatigue life *Energy* 30(11) pp 2101-2114
[8] Hillmer B, Borstelmann T, Schaffarczyk P, Dannenberg L 2007 Aerodynamic and structural design of MultiMW wind turbine blades beyond 5 MW *J Phys: Conf Ser. IOP Publishing* p 012002
[9] Liu X, Chen Y, Ye Z 2007 Optimization model for rotor blades of horizontal axis wind turbines *Front Mech Eng* 2 pp 483–8
[10] Chehouri A, Younes R, Ilinca A and Perron J 2015 Review of performance optimization techniques applied to wind turbines *Applied Energy* 142 pp 361-388
[11] Kensche C W 2006 Fatigue of composites for wind turbines *International Journal of Fatigue* 28(10) pp 1363-1374
[12] Balageas D, Fritzen CP and Güemes A. eds. 2010 Structural health monitoring 90 *John Wiley & Sons*
[13] Farrar CR and Worden K 2012 Structural health monitoring: a machine learning perspective. *John Wiley & Sons*.
[14] Adams D, White J, Rumsey M and Farrar C 2011 Structural health monitoring of wind turbines: method and application to a HAWT *Wind Energy* 14(4) pp 603-623
[15] Lambert J, Chambers A R, Sinclair I and Spearing SM 2012 3D damage characterization and the role of voids in the fatigue of wind turbine blade materials *Composites Science and Technology* 72(2) pp 337-343
[16] Mandell J F and Samborsky DD 2012 SNL/MSU/DOE Composite Material Fatigue Database *Sandia National Laboratories* Albuquerque NM
[17] Wang T 2012 A brief review on wind turbine aerodynamics *Theoretical and Applied Mechanics Letters* 2(6) pp 062001.
[18] Schubel P J and Crossley R J 2012 Wind turbine blade design review *Wind engineering* 36(4)

pp 365-388
[19] Lachenal X, Daynes S and Weaver P M 2013 Review of morphing concepts and materials for wind turbine blade applications *Wind Energy* 16(2) pp 283-307
[20] Li D, Ho S C M, Song G, Ren L and Li H 2015 A review of damage detection methods for wind turbine blades *Smart Materials and Structures* 24(3) pp 033001
[21] Wind turbine accident compilation, http://www.caithnesswindfarms.co.uk/fullaccidents.pdf
[22] Grimberg R, Tian GY, Savin A, Steigmann R and Dobrescu GS 2014 Electromagnetic Metamaterial Sensors for Structural Health Monitoring *Electromagnetic Nondestructive Evaluation* (XVII) 39 p. 3-10
[23] Xu J, Dong Y and Li H 2014 Research on fatigue damage detection for wind turbine blade based on high-spatial-resolution DPP-BOTDA. *In Sensors and Smart Structures Technologies for Civil, Mechanical and Aerospace Systems* 906130
[24] Takeda SI, Aoki Y and Nagao Y 2012 Damage monitoring of CFRP stiffened panels under compressive load using FBG sensors *Composite Structures 94*(3) pp 813-819
[25] Kuang KSC, Kenny R, Whelan MP, Cantwell WJ and Chalker PR 2001 Residual strain measurement and impact response of optical fibre Bragg grating sensors in fibre metal laminates *Smart Materials and Structures*, 10(2) pp 338.
[26] López-Higuera JM Ed 2002 *Handbook of optical fibre sensing technology* Wiley.
[27] Gouveia CA, Baptista JM and Jorge PA, 2013 Refractometric Optical Fiber Platforms for Label Free Sensing *In Current Developments in Optical Fiber Technology InTech*.
[28] Daliri A, Galehdar A, Rowe WS, Ghorbani K and John S 2012 Utilising microstrip patch antenna strain sensors for structural health monitoring *Journal of Intelligent Material Systems and Structures* 23(2) pp169-182
[29] Chen T, Li S and Sun H 2012 Metamaterials application in sensing *Sensors* 12(3) pp 2742-2765
[30] Pendry JB, Holden AJ, Robbins DJ and Stewart WJ 1999 Magnetism from conductors and enhanced nonlinear phenomena *IEEE Transactions on Microwave Theory and Techniques* 47(11) pp 2075-2084
[31] Sievenpiper D, Zhang L, Broas RF, Alexopolous NG and Yablonovitch E 1999 High-impedance electromagnetic surfaces with a forbidden frequency band *IEEE Transactions on Microwave Theory and Techniques* 47(11) pp 2059-2074
[32] Pendry JB, Holden AJ, Stewart WJ and Youngs I 1996 Extremely low frequency plasmons in metallic mesostructures *Physical Review Letters* 76(25) p 4773
[33] Savin A, Steigmann R and Dobrescu GS 2014 Metamaterial Sensors for Structural Health Monitoring *In Proceedings of the ASME 2014 12th Biennial Conference on Engineering Systems Design and Analysis, Copenhagen, Denmark* pp 25-27
[34] Vishay - Strain Gage Rosettes: Selection, Application and Data Reduction, Tech Note TN-515 http://www.vishaypg.com/docs/11065/tn-515.pdf
[35] FS22 Industrial BraggMETER HBM Germany User Manual, 2017.
[36] ASTM D5868 - 01(2014) Standard Test Method for Lap Shear Adhesion for Fiber Reinforced Plastic (FRP) Bonding.
[37] Sciammarella CA and Sciammarella FM 2012 Strain gage rosettes: selection, application and data reduction *Experimental Mechanics of Solids*, John Wiley & Sons Ltd pp111-121

Acknowledgements
This paper is partially supported by Romanian Ministry of Research and Innovation under UEFICDI Grant no PN-III-P1-1.2-PCCDI-2017-0239 and Nucleus Program PN 18 06 01 02. Authors thank to SARTOROM IMPEX Romania for funding the registration fee.